JOURNAL OF OPTOELECTRONICS AND ADVANCED MATERIALS Vol. 8, No. 5, October 2006, p. 1731 - 1735

The supplementary compression stresses in $Fe_{77.5}Si_{7.5}B_{15}$ wires

I. AŞTEFĂNOAEI[a*], D. RADU[a], H. CHIRIAC[b]
[a]*"Alexandru Ioan Cuza" University, Carol I Blvd., 11, 700506, Iasi, Romania*
[b]*National Institute of Research and Development for Technical Physics 47 Mangeron Blvd., 700050 Iasi, Romania*

The paper deals with the calculation of the internal stresses distribution in conventional amorphous wires, taking into account the supplementary mechanical stresses appearing into the wires due to the additional compression stresses exerted by the exterior shells on the inner ones during the solidification process. The consideration of these supplementary stresses leads to a better agreement between the theoretical and experimental.

(Received September 6, 2006; accepted Septemebr 13, 2006)

Keywords: Conventional amorphous wires, Rapid cooling process, Solidification process, Thermal stresses

1. Introduction

The elaboration of a theoretical model that simulate in an exact manner the magnetic domains structure of a conventional amorphous wire (CAW) is still a "serious" problem, although in the last 15 years there were published a lot of papers on this subject. In most cases, the CAW's preparation process implies the use of a glass-forming alloy [1, 2, 3]. During the solidification, due to the rapid cooling process, significant thermal gradients appear in the material leading to the appearance of residual thermal stresses in the CAW. All the previous theoretical considerations made in order to determine these stresses distribution are not taking into account the contribution of the mechanical compression exerted by the exterior shells on the inner ones.

In this paper, first we will determine the spatio-temporal temperature distribution into the CAW during the rapid solidification process. This distribution will be used in the second stage to evaluate the induced stresses by considering both the contribution of the thermal gradients appearing in the already solidified shell and the mechanical contribution (the contribution brought by the above-mentioned compression). Using this stress distribution we shall determine the magnetic domains structure of a CAW. Previous studies [4] showed that for a CAW with $\lambda > 0$, the minimization of the magnetoelastic energy arising from the coupling between internal stresses induced during rapid solidification [5] and λ (magnetostriction constant) leads to the formation of a domain structure consisting of a cylindrical inner core (IC) with a neat axial easy axis and an outer shell (OS) with radial easy axis. From the experimental data it results that the volume of the axial IC is approximately half the volume of CAW. Magnetic measurements were performed in order to verify the results obtained by theoretical considerations.

2. The solidification process of the CAW

In order to determine the internal residual stresses induced in the CAW, we have to know the spatio-temporal distribution of the temperature during the solidification process. The internal energy of the material changes due to the heat losses through conduction and the energy delivery through solidification. The samples' solidification takes place gradually, from the exterior to the interior of the molten alloy in the radial direction. According to the CAW's preparation method (in-rotating-water quenching technique), we consider that the wires exterior surface during the preparation is maintained at a constant temperature equal to the room temperature, $T_w = 300\ K$. Let us denote by $R_1 = R_1(t)$ the radius of the inner cylinder formed by the unsolidified material at a certain instant t, by $X(t)$ the "depth" (on the radial direction, from the wire's surface to its core) where the solidification front reached at the instant t, and by R_2 the radius of the wire. Obviously, $R_1(t) = R_2 - X(t)$. The solidification process begins at $t = 0$, when $X(t=0) = 0$ and $R_1(t=0) = R_2$. After a time t_s, the solidification front arrives in the CAW's center, when the whole mass of melted material is solidified. Obviously, we may write: $X(t = t_s) = R_2$, $R_1(t = t_s) = 0$. At the instant moment t, when the solidification front arrives at the surface of the cylindrical shell of radius $r = R_1(t)$, the transverse surface of the wire is divided into two distinct zones: the first one (1) corresponds to the already solidified material, while the second one (2) corresponds to the material yet unsolidified. The two zones are connected through the solidification front. We consider that the solidification

front temperature $\left(r = R_1(t)\right)$ correponds to $T_m = 1400\,K$ (the temperature of the melted material) and the material to be solidified, finally reaches the room temperature, $T_w = 300K$ .The spatio-temporal distribution of the wire's temperature is determined by the Fourier equation of the heat transport [6]:

$$c_p \rho_m \frac{\partial T}{\partial t} = \frac{1}{r}\frac{\partial}{\partial r}\left(rk\frac{\partial T}{\partial r}\right), \quad (1)$$

where $R_1(t) < r < R_2$. In eq. (1) c_p is the specific heat, ρ_m is the mass density and k is the thermal conductivity of the material [2, 5]. The solution of eq. (1) with the following boundary conditions:

$$T(R_1,\ t) = T_m,\ T(R_2,\ t) = T_w,\ T(r,\ t=0) = T_m \quad (2)$$

represents the spatio-temporal distribution of the temperature in zone (2):

$$T(r,\ t) = \pi(T_m - T_w)\sum_{j=1}^{\infty}\frac{J_0^2(\alpha_j)Z_0(\alpha_j r/R_1)\exp[-a\alpha_j^2 t/R_1^2]}{J_0^2(\alpha_j) - J_0^2(\alpha_j R_2/R_1)} + \frac{T_m \ln[R_2/r] + T_w \ln[r/R_1]}{\ln[R_2/R_1]}$$

where

$$Z_0(\alpha_j r/R_1) = N_0(\alpha_j R_2/R_1)J_0(\alpha_j r/R_1) - N_0(\alpha_j r/R_1)J_0(\alpha_j R_2/R_1)\ ,$$

$J_0(pr)$ are the first order Bessel functions, $N_0(pr)$ are the Neumann functions, $a = k/(c_p\rho_m)$, while $\alpha_j \equiv p_j R_1$ are the roots of the characteristic equation:

$$\frac{J_0(\alpha)}{J_0(\alpha\ R_2/R_1)} = \frac{N_0(\alpha)}{N_0(\alpha\ R_2/R_1)}\ .$$

3. The internal residual stresses appearing during the solidification process

3.1. The stresses due to the thermal gradients

We consider that the components of the displacement vector $\vec{u}$ of any point of the wire, namely u_r, u_θ and u_z are independent on each other. Because of the spatial symmetry of the solidification process, and implicitly of the displacements and strains generated by this process, $u_\theta = 0$ in each point of the material. Because of this, we are interested only in the radial (u_r) and axial (u_z) components of the vector $\vec{u}$. The radial temperature gradients lead to the appearance of radial (u_r^m), axial (u_z^m) and azimuthal (u_θ^m) displacements in the wire. These displacements satisfy the differential displacements' equation [7]:

$$\frac{d}{dr}\left[\frac{1}{r}\frac{d(u_r^m r)}{dr}\right] = \frac{1+\mu}{1-\mu}\alpha_m\frac{dT(r)}{dr},\ \frac{du_z^m}{dz} = const. \quad (4)$$

α_m is the CAW's thermal expansion coefficient, $\mu = 1/3$ is the Poisson's coefficient and $T(r) \equiv T(r,t)$ is the radial temperature distribution in the sample. The non-zero stress components are [8]:

$$\begin{aligned}
\sigma_{rr}^m(x,\varepsilon) &= \frac{\alpha_m E_m}{1-\mu}\frac{1}{x^2}\left\{\left[\left(x^2-\varepsilon^2\right)/\left(1-\varepsilon^2\right)\right]\int_\varepsilon^1 xT(x)dx - \int_\varepsilon^x xT(x)dx\right\} \\
\sigma_{\theta\theta}^m(x,\varepsilon) &= \frac{\alpha_m E_m}{1-\mu}\frac{1}{x^2}\left\{\left[\left(x^2+\varepsilon^2\right)/\left(1-\varepsilon^2\right)\right]\int_\varepsilon^1 xT(x)dx + \int_\varepsilon^x xT(x)dx - x^2T(x)\right\} \\
\sigma_{zz}^m(x,\varepsilon) &= \frac{\alpha_m E_m}{1-\mu}\left[\frac{2}{1-\varepsilon^2}\int_\varepsilon^1 xT(x)dx - T(x)\right]
\end{aligned} \quad (5)$$

where E_m is the Young's modulus, $\varepsilon = \varepsilon(t) = R_1(t)/R_2$ and $x = r/R_2$. The radial, azimuthal and axial stresses in a certain point x, $(0 < x < 1)$ result from the integration of (5), *i.e.*:

$$\sigma_{rr}^m(x) = \int_0^x \sigma_{rr}^m(x,\varepsilon)d\varepsilon\ ,\ \sigma_{\theta\theta}^m(x) = \int_0^x \sigma_{\theta\theta}^m(x,\varepsilon)d\varepsilon\ ,\ \sigma_{zz}^m(x) = \int_0^x \sigma_{zz}^m(x,\varepsilon)d\varepsilon \quad (6)$$

and they are presented in Fig. 1.

As one can observe from Fig. 1, the curves representing the radial and axial stresses cross at $x_{z-r}^{t.g.} = 0.72$ of the wire's radius, while the intersection of the curves representing the circumferential and radial stresses appears at $x_{\theta-r}^{t.g.} = 0.54$ of the CAW's radius; both distances were measured from the CAW's symmetry axis. So, from the perspective of the magnetic domains' structure, the stresses due only to the thermal gradients indicate the existence of an axially magnetized IC with a radius of $x_{z-r}^{t.g.} = 0.72$ of the CAW's radius and an OS with the thickness $1 - x_{z-r}^{t.g.} = 0.28$ of the radius R_2 of the wire.

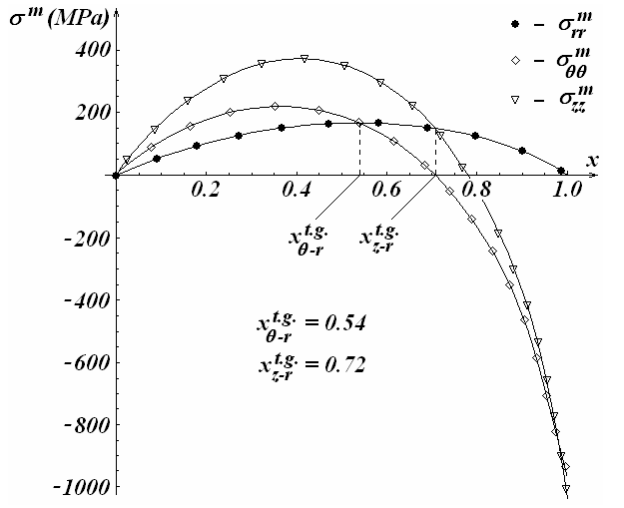

Fig. 1. The x-dependence of the stresses (radial, azimuthal and axial) due to the thermal gradients.

The thermal stresses (5) depend on the radial (r) and time variable, but in the following we focus only on the discussions regarding the radial dependences of the stresses in the time (t_s) in order to find the magnetic structure of the wire. After the time t_s when the solidification process ends, the temporal graphical representation of the stresses presents a constant palier on the time.

3.2. The stresses due to the compression of the internal shells by the external ones

Due to the radial temperature distribution in the solid shell, the thermal stresses are induced inside the shell. These stresses are given by (6). But the external solid shell compresses the inner melted part of the wire. So, during the solidification, a pressure appears at the interface between the two zones (interface that separates the melted and the solidified material); this pressure acts from the exterior to the inner shells. Using again the notations: $x \equiv r / R_2$ and $\varepsilon = \varepsilon(t) = R_1(t) / R_2$, for the supplementary stresses due to the compression one can obtain the following equations:

$$\sigma_{rr}^s(x,\varepsilon) = \frac{p\varepsilon^2}{1-\varepsilon^2}\left(1-x^{-2}\right), \sigma_{\theta\theta}^s(x,\varepsilon) = \frac{p\varepsilon^2}{1-\varepsilon^2}\left(1+x^{-2}\right)$$

$$\sigma_{zz}^s(x,\varepsilon) = \mu\frac{2p\varepsilon^2}{1-\varepsilon^2} \qquad (7)$$

By integrating, one can obtain:

$$\sigma_{rr}^s(x) = \int_0^x \sigma_{rr}^s(x,\varepsilon)d\varepsilon\ ,\ \sigma_{\theta\theta}^s(x) = \int_0^x \sigma_{\theta\theta}^s(x,\varepsilon)d\varepsilon\ ,$$

$$\sigma_{zz}^s(x) = \int_0^x \sigma_{zz}^s(x,\varepsilon)d\varepsilon\ . \qquad (8)$$

The pressure p exerted due to the solidification of the inner melted shell is determined by the compression of the whole solidified exterior shell, which is submitted to radial stresses due to the thermal gradients. In other words, we may write:

$$p \equiv p(x) = -\int_0^x \sigma_{rr}^m(x,\varepsilon)\, d\varepsilon$$

where $\sigma_{rr}^m(x,\varepsilon)$ is given by (5.1). The pressure p determined above is replaced into (7); these expressions combined with (8), give the stresses (radial, circumferential and axial) due to the compression. The total stresses in the wire are obtained from the algebric summation of the stresses due to the thermal gradients (σ^m) and those due to the compression (σ^s): $\sigma^{tot} = \sigma^m + \sigma^s$. The total stresses are shown in Fig. 2.

4. The magnetic domain structure of the CAW

As one can observe in Fig. 2, the magnetic domain structure of the CAW is affected by the consideration of the supplementary stresses due to the compression, σ_{rr}^s, $\sigma_{\theta\theta}^s$ and σ_{zz}^s. Starting from $x = 0$ up to $x_{z-r}^{tot} = 0.682$ there is a region in which $\sigma_{zz}^{tot}(x)$ is the component with the highest positive value (zone I). Then, up to $x_{oz}^{tot} = 0.75$ there is a second region, much narrower than the first one, in which $\sigma_{rr}^{tot}(x)$ is the highest positive stress component (zone II). The remaining part of the wire constitutes a third region, dominated by the negative values (compression) of $\sigma_{zz}^{tot}(x)$ and $\sigma_{\theta\theta}^{tot}(x)$ (zone III).

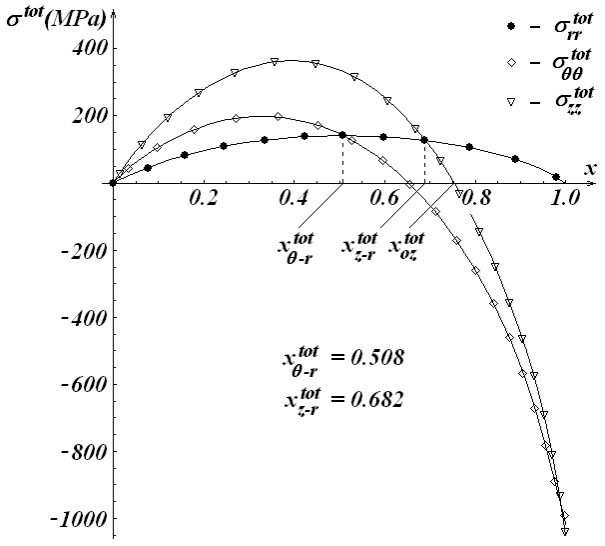

Fig. 2. The x-dependence of total stresses (thermal gradients and compression contributions).

As it is well known, the $Fe_{77.5}Si_{7.5}B_{15}$ alloy is positive magnetostrictive ($\lambda = 3\cdot 10^{-5}$). This feature leads to a strong coupling between the internal stresses and the magnetostriction, which determines the appearance of 2 distinct regions in the CAW: regions with easy axes of magnetization in which the dominant internal stresses are positive (tensile) and respectively, regions with hard axes of magnetization where the dominant stresses are negative (compressive). So, the magnetoelastic energy minimization leads to a magnetic domain structure which has the following structure:

- zone I: $x \in [0, x_{z-r}^{tot})$; due to the coupling between $\sigma_{zz}^{tot}(x)$ (positive) and the magnetostriction the first zone exhibit an uniaxial magnetic anisotropy having the easy axis oriented along the axis of the CAW (Oz - axis);
- zone II: $x \in (x_{z-r}^{tot}, x_{oz}^{tot})$; due to the coupling between $\sigma_{rr}^{tot}(x)$ (positive) and the magnetostriction the second zone has a radial magnetic anisotropy. The compressive component $\sigma_{\theta\theta}^{tot}(x)$ generates a hard axis of magnetization on the azimuthal direction;
- zone III: $x \in (x_{oz}^{tot}, 1]$; in this zone we have the two compressive components ($\sigma_{\theta\theta}^{tot}(x)$ and $\sigma_{zz}^{tot}(x)$. This zone presents a easy axis of magnetization which appears because of the coupling between the $\sigma_{rr}^{tot}(x)$ (positive) and the magnetostriction. This zone presents an azimuthal anisotropy.

Therefore, we can conclude that the stress distribution presented in Fig. 2, coupled with the positive magnetostriction of the $Fe_{77.5}Si_{7.5}B_{15}$ alloy, leads in a first order approximation to an easy axes distribution associated with a domain structure consisting of a cylindrical IC with axial magnetization (zone I) and an OS with radial magnetization (zone II plus zone III).

5. Experimental results

In order to verify experimentally the above-obtained theoretical results, we have performed magnetic measurements on $Fe_{77.5}Si_{7.5}B_{15}$ CAW by a fluxmetric method [8] in an maximum alternating field of $1700\, A/m$, at $200 Hz$. We have measured the switching field H^*, the field at which the Large Barkhausen Effect (LBE) appears, and the magnetization M^* corresponding to this field. For the considered wire, the LBE occurs at $H^* = 12 A/m$, and we have found an experimental value of the squareness $(M^*/M_s)_{\exp}$ of 0.46. Using the following relation [7]:

$$R_c / R_2 = (M^*/M_s)^{1/2},$$

we have calculated the experimental value of the fraction $x_{z-r}^{\exp} \equiv r_{z-r}^{\exp}/R_2$ as being 0.68. Thus, between the two situations (with and without considering the supplementary stresses due to the compression) there are only small quantitative differences. Nevertheless, it is worth showing the fact that, if we also consider the contribution of the component due to the compression in the final stresses, then the agreement between the experimental measurements and the theoretical results becomes very good (the relative error on the dimensions of the magnetic domains being only of 0.29%); if we neglect the mechanical contribution (the compression), then the difference between the experimental and the theoretical data increases (regarding the same relative error) to 5.9%.

5. Conclusions

We have calculated the values of the internal stresses induced on the radial, axial and azimuthal directions during the preparation process of the conventional amorphous $Fe_{77.5}B_{15}Si_{7.5}$ magnetic wires. These stresses have been calculated taking into account both the temperature gradients in the solidified material and the compression of inner shells by the external ones already solidified. The total tensile stresses have values of the order of $10^2 MPa$, while for the total compressive stresses we have obtained values of the order of $10^3 MPa$. Taking into account the high positive magnetostriction of the $Fe_{77.5}B_{15}Si_{7.5}$ alloy, the following magnetic domain structure results: (i) between $x = 0$ and $x = x_{z-r}^{tot}$ a zone with an uniaxial magnetic anisotropy, having the easy axis oriented along the axis of the CAW (Oz - axis) due to the coupling between $\sigma_{zz}^{tot}(x)$ (positive) and the magnetostriction; (ii) between $x = x_{z-r}^{tot}$ and $x = x_{oz}^{tot}$ a zone with a radial magnetic anisotropy due to the coupling between $\sigma_{rr}^{tot}(x)$ (positive) and the magnetostriction. Also, in this zone the compressive component $\sigma_{\theta\theta}^{tot}(x)$ generates a hard axis of magnetization on the azimuthal direction; (iii) finally, between $x = x_{oz}^{tot}$ and $x = 1$ we have a zone with two compressive components ($\sigma_{\theta\theta}^{tot}(x)$ and $\sigma_{zz}^{tot}(x)$, respectively). Also, this zone shows azimuthal anisotropy. Taking into consideration the supplementary stresses due to the compression of the inner shells by the solidified external ones, a very good agreement between the theoretical and experimental results is achieved (the relative error on the magnetic domains sizes being of only 0.29%); if these supplementary stresses are not taken into account (considering only the stresses due to the thermal gradients, the relative error is approaching 6%.

Acknowledgement

The authors wish to thank Romanian CEEX POSTDOC-NANOSCIENCE for the financial support of this research.

References

[1] M. Hagiwara, A. Inoue, "Production Techniques of Alloy Wires by Rapid Solidification in Rapidly Solidified Alloys", edited by H.H. Liebermann, Marcel Dekker, New York, 1993, p. 141.
[2] H. Chiriac, T.A. Óvári and Gh. Pop, Phys. Rev., B **52**(14), 10104 (1995).
[3] M. Vázquez, C. Gómez-Polo, D.X. Chen, A. Hernando, IEEE Trans. Magn. **30**, 907 (1994).
[4] H. Chiriac, E. Hristoforou, Maria Neagu, I. Darie, Mat. Sci. Eng., A **304-306**, 1011 (2001).
[5] H. Chiriac, T. A. Óvári, Prog. Mater. Sci. **40**(5), 333 (1996).
[6] P. J. Schneider, Conduction Heat Transfer, Addison Wesley Publishing Company Inc., 1955.
[7] B. A. Bosley, J. H. Weiner, Theory of Thermal Stresses, Wiley, New York, 1960, pag. 291.
[8] K. Mandal, S. K. Ghatak, J. Magn. Magn. Mater. **118**, 315 (1993).

*Corresponding author: iordana@uaic.ro